Metals & corrosion

Thermodynamic and diffusion kinetic studies of the Co-Al–Fe system

Jingjing Wang[1,2], Yu Zhang[2], Weisen Zheng[1,*] , and Xiao-Gang Lu[1,3,*]

[1] *School of Materials Science and Engineering, Shanghai University, Shanghai 200436, China*

[2] *Ansteel Beijing Research Institute Co., Ltd, Beijing 102200, China*

[3] *Materials Genome Institute, Shanghai University, Shanghai 200072, China*

ABSTRACT

The Co-Al–Fe system has attracted extensive interests as a core system in Co-based alloys and high-entropy alloys. In the present work, a thermodynamic assessment of the Co-Al–Fe system and atomic mobility of its face-centered cubic (fcc) phase were performed with the CALPHAD method. To supplement the phase boundary of the B2 phase at the Al-rich side and clarify the miscibility gap of the B2 phase in the Co-Al–Fe system, the Al-rich phase boundary of the ordered body-centered cubic (bcc) phase (B2) at 1273 and 1343 K, as well as the phase equilibria at the Co-Fe-rich side at 1073 K, was determined using electron probe microanalysis (EPMA) and X-ray diffraction (XRD) analysis. Combined with the experimental data from the literature, the thermodynamic description of the Co-Al–Fe system was established. The model parameters can reproduce the most reliable phase diagram data. In addition to the thermodynamic study, the interdiffusion coefficients in the face-centered cubic (fcc) phase of the Co-Al–Fe system were experimentally deduced from the composition profiles of 20 diffusion couples at 1323, 1423, and 1523 K. Based on the thermodynamic description and experimental diffusivities, the atomic mobilities of Co, Al, and Fe in fcc Co-Al–Fe alloys were assessed. A comprehensive comparison between the calculated results and experimental data indicates excellent agreement between the diffusion paths and composition profiles.

Introduction

The Co-Al–Fe system is a critical subsystem of high-temperature Co-based alloys and promising high-entropy alloys (HEAs) for extensive applications. HEAs comprise simple phase constitutions, such as disordered face-centered cubic (fcc) phase, disordered body-centered cubic (bcc) phase (i.e., A2), and ordered bcc phase (i.e., B2) and exhibit excellent mechanical properties [1–5]. Screening alloy compositions and designing industrial processes, such as

---

⧉ Springer

homogenization and heat treatments, have been effectively accelerated by computational techniques based on thermodynamic and kinetic databases of alloys. Therefore, the establishment of a thermodynamic database of the Co-Al–Fe system and mobility database for major constituting phases (e.g., fcc) is essential.

The main objectives of this study are as follows: (i) determine the phase boundary of the B2 phase at the Al-rich side at 1273 and 1343 K and the phase equilibria at the Co-Fe side at 1073 K; (ii) obtain a comprehensive assessment of the thermodynamic properties of the Co-Al–Fe system; (iii) measure the interdiffusion coefficients in the fcc phase at 1323, 1423, and 1523 K, and (iv) establish the atomic mobilities of Co, Al, and Fe in fcc Co-Al–Fe alloys.

Literature review

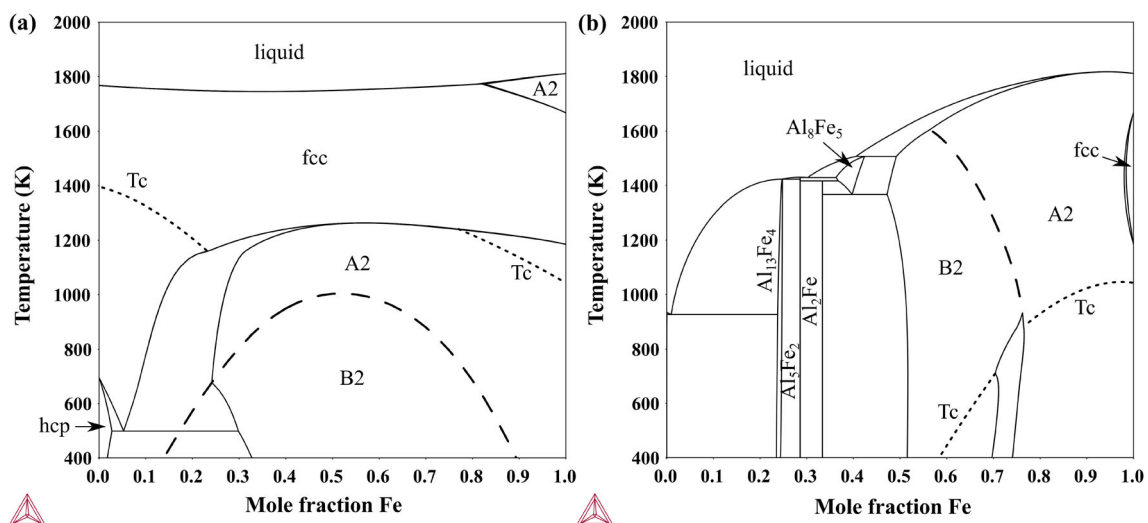### Thermodynamics and phase diagram

Binary systems

Thermodynamic evaluation of the Co-Al binary system has been performed many times [6–13]. The first complete assessment of the binary system was made by Dupin and Ansara [6]. Stein et al. [8] measured the homogeneity range of the B2 phase and re-assessed the binary system. The thermodynamic description can reproduce the available experimental data well. However, there is an inverse miscibility gap of the liquid phase at high temperature. Later, Liu et al. [9]

modified the model parameters of the B2 phase based on the thermodynamic description by Dupin and Ansara [6]. However, the experimental data, such as liquidus [8], were not considered. Based on a thorough review of the Co-Al, Wang et al. [10] presented a new description of the Co-Al system, particularly for the complex $Al_{13}Co_4$ phases; nevertheless, the calculated melting point of the B2 phase was slightly higher than the experimental data [8]. More recently, Wang et al. [11], Ostrowska and Cacciamani [12], and Noori and Hallstedt [13] made some modifications of the model parameters based on the previous thermodynamic descriptions, respectively. In fact, Wang [14], in our research group, modified the thermodynamic parameters of the liquid, fcc, A2 and B2 phases to reproduce the liquidus around the B2 phase based on the description from Stein et al. [8]. The thermodynamic description was successfully applied to a quinary Ni-Co-Al-Mo-W system. However, the sublattice model for the $Al_{13}Co_4$ phase is not consistent with that for the $Al_{13}Fe_4$ phase. To maintain the consistency of thermodynamic models in the Co-Al–Fe system, the modification of the Co-Al system was performed in the present study.

Most recently, the Co-Fe system was comprehensively assessed by the present authors [15]. The experimental data were well reproduced by the thermodynamic description, which was adopted in the present work. The calculated Co-Fe phase diagram is shown in Fig. 1a.

The most widely accepted assessment of the Al–Fe system was established by Sundman et al. [16]. Zheng

Figure 1 Assessed binary phase diagrams: **a** Co-Fe [15], and **b** Al–Fe [17].

et al. [17] re-assessed the system to reproduce the experimental integral enthalpy of mixing of the liquid phase. Thus, the thermodynamic description by Zheng et al. [17] was adopted in this study. The calculated Al–Fe phase diagram is shown in Fig. 1b.

Co–Al–Fe ternary system

Recently, the phase equilibria at the Co-Fe-rich side of the ternary Co–Al–Fe system at 1173, 1273, 1373, and 1473 K were carefully studied in our previous work [18], in which most experimental data in the literature were reviewed and discussed. Thus, only the unmentioned key experimental data are reviewed here in detail. Raynor and Waldron [19] investigated the vertical sections across the Al-rich corner ($\geq$ 97.5 wt.% Al) including liquidus through thermal analysis; however, these data were not used in the present assessment due to uncertain accuracy. Ackermann [20] measured the phase equilibria on the Co-Fe rich side at temperatures between 1073 and 1473 K using diffusion couples. The miscibility gap of the bcc phase was also studied at 923 K. Most recently, Zhu et al. [21] constructed three complete isothermal sections at 1073, 1173, and 1273 K based on the results obtained from three identical $Co/Fe/Al_5Fe_2$ diffusion triples and ternary alloys using scanning electron microscopy (SEM), electron probe microanalysis (EPMA), and X-ray diffraction (XRD). The experimental results for the Co-Fe-rich side at 1173 and 1273 K are consistent with the results of the present authors [18]. Earlier, Grushko et al. [22] determined a partial isothermal section with more than 55 at.% Al at 1073 and 1343 K by means of SEM, energy dispersion spectroscopy (EDS) and powder XRD, focusing on the structure of Al-rich compounds and their equilibria with B2 phase.

Ostrowska and Cacciamani [12] performed a thermodynamic assessment of the Co–Al–Fe system. However, their work had limitations. First, the phase boundary of Al-rich compounds was established with a large error owing to insufficient experimental data. More importantly, the phase relationship at the Co-Fe side at 1173 and 1273 K does not agree with the experimental results of Wang et al. [18] and Zhu et al. [21]. Furthermore, the $L2_1$ phase structure for the first-principles calculations was confused with the B2 phase. In addition, according to the prediction obtained by Ostrowska and Cacciamani [12], there exists a miscibility gap of the B2 phase and a two-phase region (A2 + B2) at the Co-Fe side at 1073 K, which was not confirmed by the experimental isothermal section determined by Zhu et al. [21]. However, in the work of Zhu et al. [21], the interface Co/Al_5Fe_2 of the diffusion triple was badly bonded. Therefore, more experimental work at 1073 K is required to clarify the miscibility gap of the B2 phase. Recently, Noori and Hallstedt [23] re-assessed the Co–Al–Fe system, focusing on the magnetic transition of the B2 phase. However, the thermodynamic calculations indicate that the miscibility gap of the B2 phase is stable at 1073 and 1173 K, which may be attributed to the fitting with the experimental data at 923 K.

Diffusion data

Wang [14] in our research group optimized the atomic mobilities for the fcc phase in the Co-Al system based on the updated thermodynamic description. The diffusion behavior was well described using mobility parameters [14]. The atomic mobilities in fcc Co-Fe alloys were assessed by the present authors [15] and were used in this work. As the composition range of the fcc phase in the Al–Fe system is very narrow, no binary interaction parameter is required. The parameters for impurity diffusion for Al in fcc-Fe and Fe in fcc-Al were adopted from the works of Du et al. [24] and Liu et al. [25], respectively, in view of their good consistency with experimental data. For the ternary Co–Al–Fe system, no interdiffusion coefficients and mobility assessment for the fcc phase have been reported to date.

Thermodynamic and atomic mobility models

Thermodynamic models

Substitutional solution phases

Except for the hexagonal close-packed (hcp) phase at low temperatures, three solution phases, liquid, fcc, and bcc, were considered in the present assessment. The total molar Gibbs energy of the solution phase can be described by the following equation:

$$G_m^{\varphi} = x_{Al}{}^oG_{Al}^{\varphi} + x_{Co}{}^oG_{Co}^{\varphi} + x_{Fe}{}^oG_{Fe}^{\varphi}$$
$$+ RT(x_{Al}\ln x_{Al} + x_{Co}\ln x_{Co} + x_{Fe}\ln x_{Fe}) + {}^{ex}G_m^{\varphi}$$
$$+ {}^{mag}G_m^{\varphi}$$

$$(1)$$

where R and T are the gas constant and absolute temperature, respectively. x_{Al}, x_{Co}, and x_{Fe} are the mole fractions of Al, Co, and Fe, respectively. The term ${}^{ex}G_m^{\varphi}$ is the excess Gibbs energy and is described by the Redlich–Kister polynomials [26]. The magnetic contribution ${}^{\varphi}G_m^{mag}$ to the total Gibbs energy of the fcc and bcc phases is included. The model of magnetic contribution was proposed by Inden [27] and later simplified by Hillert and Jarl [28].

Ordered B2 phase

The ordered bcc phase (B2) was considered in the present assessment. Considering the consistency of the thermodynamic model of the B2 phase, the model used by Zheng et al. [17] was modified by introducing a vacancy into the sublattice, that is, $(Al,Co,Fe,Va)_{0.5}(Al,Co,Fe,Va)_{0.5}$. The addition of the interaction parameter between the vacancy and metal atom has almost no influence on the Gibbs energy of the disordered bcc and ordered B2 phase in the Al–Fe system. Ansara et al. [29] proposed a partitioning model to consider the A2/B2 order–disorder transition. The model can describe both disordered bcc and ordered B2 phase with a single Gibbs energy function that is composed of the disordered state and the ordering contribution part. This relationship can be described as follows:

$$G_m^{ord} = G_m^{dis}(x_i) + \Delta G_m^{ord}(y_i^s)$$
$$= G_m^{dis}(x_i) + G_m^{ord}(y_i^s) - G_m^{ord}(y_i^s = x_i)$$

$$(2)$$

where y_i^s is the fraction of component i in the sublattice s. The first term $G_m^{dis}(x_i)$ is the Gibbs energy of the disordered bcc phase. The second term ΔG_m^{ord} is the long-range ordering contribution to Gibbs energy. The site fractions of i in the two sublattices are equal if phase B2 becomes completely disordered, that is, $y_i' = y_i'' = x_i$; for ordered B2, $y_i' \neq y_i''$.

Intermetallic compounds

According to experimental information [21, 22, 30], no new ternary phase forms in the Co-Al–Fe system. The binary intermetallic compounds are listed in Table 1. To consider the solubility of Fe or Co in the binary intermetallic compounds, Fe or Co atoms were introduced into the Co or Fe sites because of their chemical similarity. For example, the Gibbs energy of $Al_{13}(Co,Fe)_4$, modeled as $(Al)_{0.6275}(Co,Fe)_{0.235}(Al,Va)_{0.1375}$, is expressed as follows:

$$G_m^{Al_{13}(Co,Fe)_4} = y_{Co}''y_{Al}'''{}^oG_{Al:Co:Al} + y_{Co}''y_{Va}'''{}^oG_{Al:Co:Va}$$
$$+ y_{Fe}''y_{Al}'''{}^oG_{Al:Fe:Al} + y_{Fe}''y_{Va}'''{}^oG_{Al:Fe:Va}$$
$$+ 0.235RT(y_{Co}''\ln y_{Co}'' + y_{Fe}''\ln y_{Fe}'')$$
$$+ 0.1375RT(y_{Al}'''\ln y_{Al}'''y_{Va}'''\ln y_{Va}''')$$
$$+ y_{Co}''y_{Fe}''y_{Al}'''{}^0L_{Al:Co,Fe:Al}$$

$$(3)$$

where y_i'' and y_i''' are the site fractions of component i on the second and third sublattice, respectively. In the present work, the parameters ${}^oG_{Al:Co:Al}$ and ${}^oG_{Al:Co:Va}$ were optimized based on the experimental data in the binary Co-Al system in order to maintain the consistency of thermodynamic models in the ternary system. The term ${}^0L_{Al:Co,Fe:Al}$ is the ternary interaction parameter to be optimized.

Atomic mobility model

The concept of atomic mobility to model diffusivities for multicomponent systems was proposed by Andersson and Ågren [31]. For the fcc phase, the effect of magnetism is not considered, and the atomic

Table 1 Intermetallic compounds at the Al-rich corner in the Co-Al–Fe system

Phase	Prototype	Pearson symbol	Thermodynamic model
Al_9Co_2	–	$mP22$	$(Al)_9(Co,Fe)_2$
$Al_{13}(Co,Fe)_4$	–	$mC102$	$(Al)_{0.6275}(Co,Fe)_{0.235}(Al,Va)_{0.1375}$
Al_3Co	–	–	$(Al)_3(Co,Fe)_1$
Al_5Co_2	Al_5Co_2	$hP28$	$(Al)_5(Co,Fe)_2$
Al_2Fe	Al_2Fe	$aP18$	$(Al)_2(Co,Fe)_1$
Al_5Fe_2	–	$oC24$	$(Al)_5(Co,Fe)_2$
Al_8Fe_5	Cu_5Zn_8	$cI52$	$(Al,Co,Fe)_8(Al,Co,Fe)_5$

mobility M_i of the diffusing component i can be divided into an activation energy Q_i and a frequency factor M_i^0 and is expressed as follows:

$$M_i = M_i^0 \exp\left(\frac{-Q_i}{RT}\right)\frac{1}{RT} = \exp\left(\frac{\Phi_i}{RT}\right)\frac{1}{RT} \qquad (4)$$

where R and T are the gas constant and absolute temperature, respectively. Both M_i and Q_i are considered to depend on composition and temperature. In the DICTRA notation, $-Q_i$ and $RT \ln M_i^0$ can be grouped into a single parameter, Φ_i, and expressed by the Redlich–Kister polynomial [26]:

$$\Phi_i = \sum_p x_p \Phi_i^p + \sum_p \sum_{q>p} x_p x_q \left[\sum_{r=0}^r {}^r\Phi_i^{p,q}\left(x_p - x_q\right)^r\right] \qquad (5)$$

where x_p and x_q are the mole fractions of components p and q, respectively. Φ_i^p represents the value Φ_i for component i diffusing in the pure component p, and $\Phi_i^{p,q}$ represents the interaction parameter.

Experiments

Phase equilibrium experiments

To determine the phase equilibria of the Co–Al–Fe system, 12 Al-rich alloys and 18 Co-Fe rich allo1ys were designed and prepared from high-purity Al (99.99 wt.%), Co (99.98 wt.%), and Fe (99.99 wt.%)

plates by arc melting in a high-purity Ar atmosphere. The ingots were melted six times to achieve homogeneity. In sequence, the ingots were sealed in quartz tubes with purified Ar atmosphere for the subsequent annealing treatment at 1273 K/100 h for the Al-rich alloys and 1473 K/72 h for the Co-Fe-rich alloys. Subsequently, the Al-rich alloys (labeled QA1 − 12) were annealed at 1273 K for 392 h and at 1343 K for 336 h, whereas the Co-Fe-rich alloys (labeled QB1 − 18) were annealed at 1073 K for 1344 h. After grinding and polishing using standard metallographic techniques, the chemical compositions of the individual phases were determined using EPMA. The phase compositions were identified by XRD using a D/MAX2500V + /PC instrument (40 kV, 250 mA), with a Cu radiation source. Further experimental details are indicated in a previous study [18].

Interdiffusion coefficient measurements

Nineteen diffusion couples were designed to measure the interdiffusion coefficient and annealed at 1323, 1423, and 1523 K, as listed in Table 2. The alloys were prepared in the same manner as in the phase equilibrium experiments. The ingots were then cut into blocks with dimensions of 6mm × 6mm × 6mm using wire-electrode cutting. Each block was ground and polished to obtain a mirror-like surface. Then, the two corresponding blocks were bound together using a specially fabricated Mo clamp to assemble the

Table 2 Diffusion couples and experimental conditions for interdiffusion coefficient measurements

Diffusion couple	Nominal composition (at.%)	T (K)	Time (h)
FA1	Co/Co-6Al-20Fe	1323	120
FA2	Co/Co-8Al-8Fe		
FA3	Co-5Fe/Co-5Al		
FA4	Co-10Fe/Co-9Al		
FA5	Co-15Fe/Co-8Al-8Fe		
FA6	Co-20Fe/Co-6Al-20Fe		
FA7	Co-25Fe/Co-8Al-8Fe		
FB1	Co/Co-6Al-20Fe	1423	48
FB2	Co/Co-8Al-8Fe		
FB3	Co-10Fe/Co-9Al		
FB4	Co-15Fe/Co-8Al-8Fe		
FB5	Co-25Fe/Co-8Al-8Fe		
FC1	Co/Co-6Al-20Fe	1523	24
FC2	Co/Co-8Al-8Fe		
FC3	Co-5Fe/Co-5Al		
FC4	Co-10Fe/Co-9Al		
FC5	Co-15Fe/Co-8Al-8Fe		
FC6	Co-20Fe/Co-6Al-20Fe		
FC7	Co-25Fe/Co-8Al-8Fe		

desired diffusion couples. The assembled diffusion couples for interdiffusion coefficient measurements were encapsulated in quartz tubes. After the annealing treatment, the couples were quenched in water and cut parallel to the diffusion direction. After grinding and polishing, the composition-distance profiles of the diffusion couples were measured using EPMA. The interdiffusion coefficients in the fcc phase of the ternary system were determined using the Whittle–Green method [32].
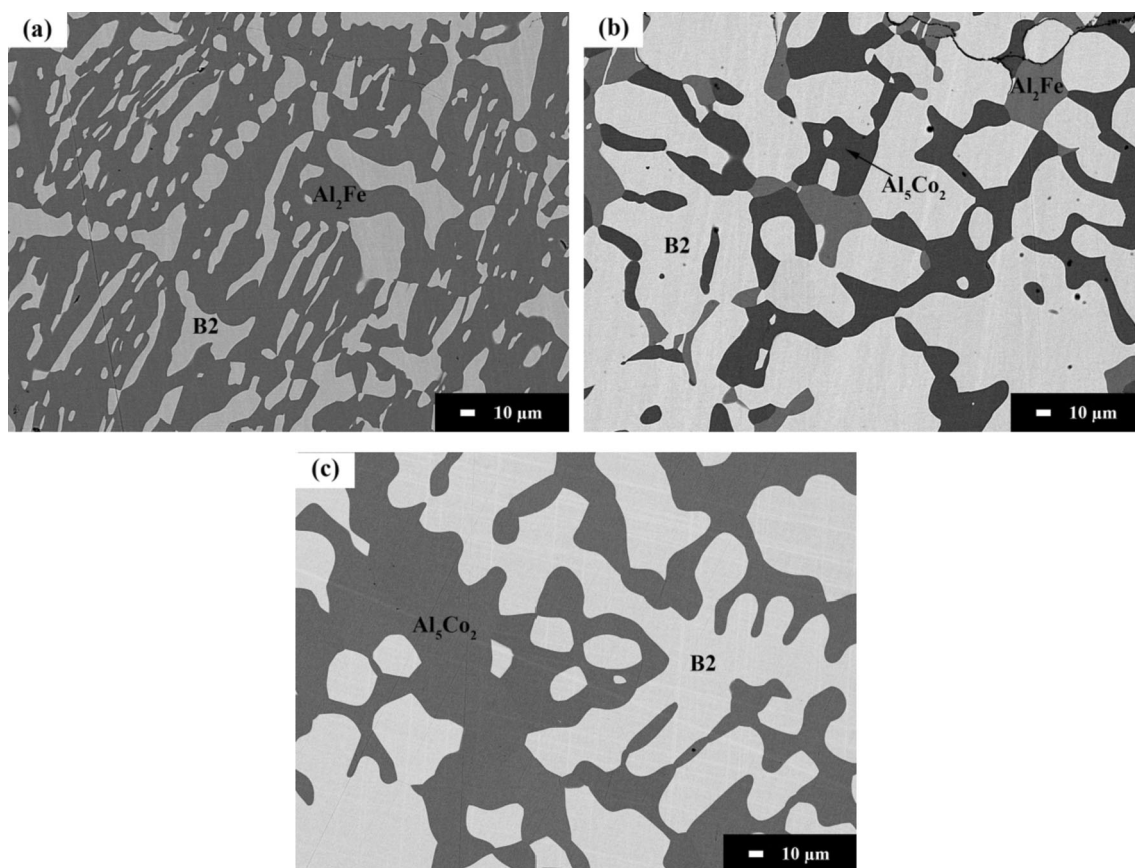
Experimental results

Phase equilibria in the Co-Al–Fe system

To determine the phase boundary of the B2 phase at the Al-rich side, the phase equilibria between the B2 phase and Al-rich intermetallic compounds were examined by annealing the alloys at 1273 and 1343 K.

Typical backscatter secondary electron (BSE) micrographs and XRD patterns of the alloys are shown in Figs. 2 and 3, respectively. The chemical compositions of the individual phases were measured using EPMA, as listed in Table 3. According to the XRD and EPMA results, the dark, gray and bright regions correspond to the Al_5Co_2, Al_2Fe, and B2 phases, respectively. No ternary compounds were observed in this study. The Al_5Co_2 phase dissolved up to 21.50 at.% Fe, whereas the Al_2Fe phase dissolved small amounts of Co. The Al content in the B2 phase remained almost unchanged.

To clarify the calculated miscibility gap of the B2 phase by Ostrowska and Cacciamani [12] and Noori and Hallstedt [23], Co-Fe rich alloys were annealed at 1073 K for 1032 h to establish the phase equilibria relationship. The chemical compositions of the individual phases are summarized in Table 4. Typical BSE micrograph of the two-phase fcc + B2 microstructure is shown in Fig. 4. According to the

Figure 2 BSE images of the alloys at the Al-rich corner: **a** QA2 at 1273 K, **b** QA3 at 1273 K, and **c** QA11 at 1343 K.
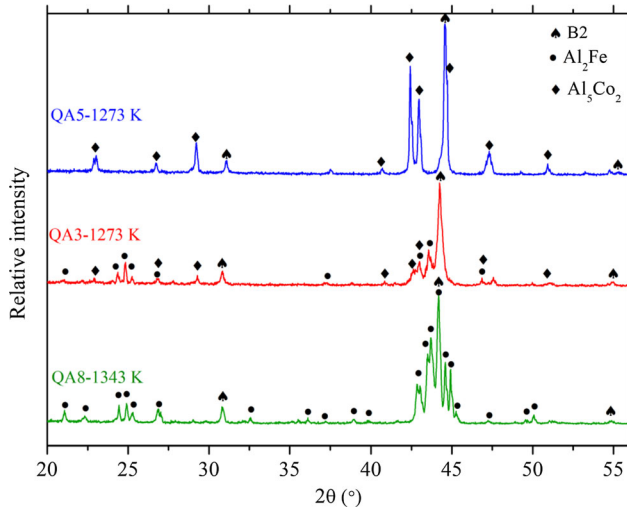
Figure 3 XRD results of alloys QA5 and QA3 at 1273 K and QA8 at 1343 K.

interdiffusion coefficients. The interdiffusion coefficients and compositions at the intersecting points of the diffusion paths of Co-Al–Fe diffusion couples determined in the present study are listed in Table 5. All interdiffusion coefficients fulfilled the thermodynamic constraints for ternary diffusion coefficients [34]. The main interdiffusion coefficients, $\tilde{D}_{AlAl}^{Co}$ and $\tilde{D}_{FeFe}^{Co}$, were always positive. $\tilde{D}_{AlAl}^{Co}$ was larger than $\tilde{D}_{FeFe}^{Co}$. The cross interdiffusion coefficients, $\tilde{D}_{AlFe}^{Co}$ and $\tilde{D}_{FeAl}^{Co}$, were either positive or negative and smaller than the main interdiffusion coefficients by one order of magnitude. Additionally, the cross interdiffusion coefficient data were more scattered than the main interdiffusion coefficients. A lower weight was assigned during mobility optimization.

Thermodynamic and mobility assessment

Thermodynamic assessment

Before the assessment of the ternary Co-Al–Fe system, the thermodynamic description of the binary Co-Al system was modified based on the assessment by Wang [14] due to the inconsistent models for the $Al_{13}Co_4$ and $Al_{13}Fe_4$ phases. The thermodynamic model for the $Al_{13}Co_4$ phase changed from $(Al)_{13}(Co)_4$ to $(Al)_{0.6275}(Co,Fe)_{0.235}(Al,Va)_{0.1375}$. The two endmember parameters were adjusted to fit the experimental phase diagram. Moreover, the thermodynamic parameters for the Al_3Co phase had to be slightly modified to reproduce the reaction of

binary phase diagram and experimental phase equilibria reported by Edwards [33] and Zhu et al. [21], the dark area corresponds to the fcc phase, whereas the bright area corresponds to the B2 phase. The two-phase boundary showed good agreement with previous experimental data [21, 33]. Additionally, the second fcc phase (fcc′) found by Edwards [33] was not detected in the present work, which agrees with the experimental observation in the work of Zhu et al. [21].

Determination of interdiffusion coefficients

The experimental composition profiles of the diffusion couples were smoothed and analyzed using the Whittle–Green method [32] to deduce the

Table 3 Experimental chemical compositions of individual phases at the Al-rich corner

T (K)	Alloy	Phase 1 (at.%)			Phase 2 (at.%)			Phase 3 (at.%)		
		Co	Al	Fe	Co	Al	Fe	Co	Al	Fe
1273	QA1	3.35	50.77	45.88	1.43	63.56	35.01	/	/	/
	QA2	6.50	50.82	42.68	2.82	63.89	33.29	/	/	/
	QA3	15.64	51.10	33.26	6.81	65.02	28.16	9.56	68.95	21.50
	QA4	25.77	50.98	23.26	/	/	/	13.98	69.38	16.65
	QA5	36.76	50.41	12.83	/	/	/	19.23	69.76	11.01
	QA6	45.99	50.17	3.84	/	/	/	25.43	70.06	4.51
1343	QA7	3.74	50.97	45.29	1.82	63.84	34.34	/	/	/
	QA8	6.81	51.15	42.03	3.23	64.36	32.42	/	/	/
	QA9	15.27	52.14	32.59	/	/	/	/	/	/
	QA10	24.43	52.57	23.00	/	/	/	14.17	69.44	16.39
	QA11	33.72	52.44	13.84	/	/	/	18.84	70.00	11.16
	QA12	45.03	51.21	3.76	/	/	/	/	/	/

**Table 4** Experimental chemical compositions of individual phases at 1073 K at the Co-Fe side

Alloy	Phase 1 (at.%)			Phase 2 (at.%)		
	Co	Al	Fe	Co	Al	Fe
QB1	77.97	4.58	17.45	60.61	17.11	22.28
QB2	76.94	6.33	16.73	60.47	18.87	20.66
QB3	84.57	5.15	10.28	59.53	29.24	11.23
QB4	62.31	12.51	25.19	76.02	4.95	19.04
QB5	79.84	4.95	15.22	59.13	25.04	15.83
QB6	66.45	3.33	30.22	/	/	/
QB7	50.71	19.21	30.09	/	/	/
QB8	56.07	29.01	14.92	/	/	/
QB9	51.88	25.68	22.45	/	/	/
QB10	64.55	5.17	30.28	/	/	/
QB11	52.43	25.16	22.40	/	/	/
QB12	46.30	18.84	34.86	/	/	/
QB13	50.58	4.91	44.51	/	/	/
QB14	52.12	34.91	12.98	/	/	/
QB15	5.30	14.94	79.76	/	/	/
QB16	10.83	18.63	70.54	/	/	/
QB17	17.28	12.22	70.50	/	/	/
QB18	54.89	5.28	39.83	/	/	/

liquid + $Al_3Co \leftrightarrow Al_{13}Co_4$. Additionally, it was found that the B2 phase assessed by Wang [14] led to a high stability for the B2 phase in the Co-Al–Fe system. Therefore, the model parameters for the B2 phase were slightly modified. The thermodynamic parameters of the Co-Al system modified in the present work are listed in Table 6. The calculated Co-Al phase diagram is shown in Fig. 5, together with the experimental data [8, 35–45].

Combined with the binary Co-Fe [15] and Al–Fe [17], the thermodynamic parameters of the Co-Al–Fe ternary system were optimized using the PARROT module in the Thermo-Calc software [46] and are listed in Table 6.

According to the thermodynamic calculations by Ostrowska and Cacciamani [12] and Noori and Hallstedt [23], an attempt to fit the miscibility gap of the B2 phase at 923 K leads to the stable existence of the miscibility gap at 1073 K or even higher temperatures. However, the recent experimental works of Zhu et al. [21] and Wang et al. [18], as well and the present work, did not find a miscibility gap. Thus, the miscibility gap of the B2 phase at 923 K was not considered unless new experimental data were available. The calculated isothermal sections for the Co-Al–Fe system were compared with the experimental data over the temperature range of 1073–1473 K, as shown in Fig. 6. As shown in Fig. 6a, the experimental phase boundaries at the Co-rich corner [21, 22, 33] were well fitted, except for a small discrepancy in the fcc phase boundary, which was inherited from the Co-Al binary description. A narrow A2 + B2 two-phase region formed at the Co-rich corner and changed to a second-order phase transition with increasing Fe content. Note that, there was no miscibility gap in the B2 phase formed in the present calculation, which is in good agreement with the experimental data.

Good agreement with experimental data [18, 21, 22, 47, 48] was also observed in the phase equilibria at the Co-Fe side in the range of 1173–1473 K, as shown in Figs. 6b–f. In this temperature range, only a second-order transition was
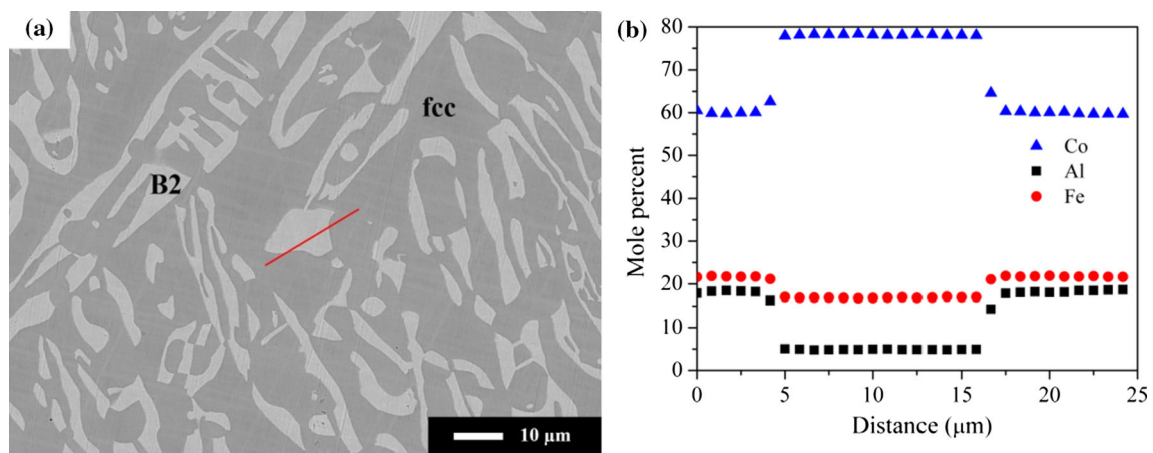
Figure 4 **a** BSE image and **b** composition profile at the phase boundary of alloy QB3 annealed at 1073 K.

Table 5 Experimental interdiffusion coefficients for the fcc Co-rich alloys

T (K)	Diffusion couple	Composition (at.%)		Interdiffusion coefficients (10^{-15} m^2/s)			
		Al	Fe	$\tilde{D}_{AlAl}^{Co}$	$\tilde{D}_{AlFe}^{Co}$	$\tilde{D}_{FeFe}^{Co}$	$\tilde{D}_{FeAl}^{Co}$
1323	FA1 − FA3	1.95	3.43	1.61	− 0.04	0.71	− 0.19
	FA1 − FA4	2.92	7.40	2.11	− 0.02	0.92	− 0.49
	FA1 − FA5	3.61	11.63	2.91	0.15	1.00	0.14
	FA1 − FA7	4.05	15.71	2.96	0.14	1.21	0.01
	FA2 − FA3	3.02	1.77	1.99	− 0.27	0.87	− 0.05
	FA2 − FA4	4.73	4.65	2.68	0.17	1.03	− 0.24
	FA6 − FA7	2.70	19.86	3.08	0.16	1.35	0.05
1423	FB1 − FB3	2.37	8.88	11.31	0.46	3.96	− 1.21
	FB1 − FB4	2.80	12.12	11.68	0.64	4.61	− 2.77
	FB1 − FB5	3.57	16.68	15.32	0.43	5.92	− 1.67
	FB2 − FB3	4.55	5.18	17.41	1.90	4.66	2.24
1523	FC1 − FC3	1.55	2.26	86.56	− 6.08	22.92	− 5.94
	FC1 − FC4	2.71	8.09	63.18	4.70	24.38	− 0.34
	FC1 − FC5	3.37	12.55	81.22	4.32	27.53	− 8.86
	FC1 − FC7	4.00	16.82	91.57	8.91	28.21	− 2.20
	FC2 − FC3	2.01	0.87	62.95	− 12.78	21.18	− 1.10
	FC2 − FC4	4.61	4.77	69.20	8.30	24.39	4.51
	FC6 − FC7	2.91	20.26	73.56	2.60	18.20	− 4.95

observed between the A2 and B2 phases, and the two-phase fcc + B2 and fcc + A2 boundaries presented inflection at the order/disorder transformation.

At the Al-rich corner, most intermetallic compounds were treated with a fixed Al content for simplification in view of the experimental facts of narrow composition ranges, except for the Al$_{13}$(Co,Fe)$_4$ phase. As observed from Figs. 5a–d, the calculated results are in agreement with the experimental data by Zhu et al. [21], and a relatively large discrepancy with the results by Grushko et al.[22] is noticeable. This discrepancy may be caused by the relatively low accuracy of the EDS composition analysis.

In the Co-Al–Fe system, the liquidus on the Co-Fe side has been rarely studied. The only available data were determined experimentally by Köster [49]. Although no ternary interaction parameters were introduced, the calculated liquidus was in good agreement with the experimental data by Köster [49], as shown in Fig. 7. As for the equilibrium between the fcc and B2 phases, the calculated results showed a certain deviation from the experimental data at 20

and 40 wt.% Fe. Considering the good agreement of the isothermal sections discussed above, this deviation may be due to experimental error.

The calculated isoplethal sections of the Co-Al–Fe system at 40 at.% Fe, 50 at.% Fe, and 50 at.% Co were compared with the experimental data [18, 47, 50, 51], as shown in Fig. 8. The calculated order–disorder transition was in good agreement with the experimental data by Wang et al. [18], as shown in Fig. 8a and b, but slightly deviated from the data by Kamyia et al. [47]. In Fig. 8c, the experimental phase equilibria by Kogachi et al. [50] were reasonably reproduced using the present thermodynamic description.

The calculated isoplethal sections at high Al contents (97.5, 98.5, and 98.75 wt.% Al) are shown in Fig. 9. The only experimental data of the phase equilibria between the liquid and intermetallic phases were reported by Raynor and Waldron [19]. The difference between the presently calculated results and the experimental data was large, particularly for the liquidus temperature. This might be attributed to the low accuracy of the experimental data. For instance, the measured liquidus temperatures of binary Fe-97.5Al (wt.%) were apparently higher than

Table 6 Thermodynamic parameters of the Co-Al–Fe system

| Phase	Parameter (J/mole per formula unit)	Reference
liquid	$^0L_{Al,Co}^{liquid} = -150510 + 33.73T$	[14]
$(Al,Co,Fe)_1$	$^1L_{Al,Co}^{liquid} = -29294.9 + 12.05T$	[14]
	$^2L_{Al,Co}^{liquid} = +33074.5 - 3.41T$	[14]
	$^0L_{Al,Fe}^{liquid} = -81930 + 16.03T$	[17]
	$^1L_{Al,Fe}^{liquid} = -15100 + 9.38T$	[17]
	$^2L_{Al,Fe}^{liquid} = +196$	[17]
	$^0L_{Co,Fe}^{liquid} = -9939 + 3.29T$	[15]
	$^1L_{Co,Fe}^{liquid} = -1713 + 0.91T$	[15]
	$^2L_{Co,Fe}^{liquid} = +1271$	[15]
bcc	$^0L_{Al,Va}^{A2} = +160000 - 31T$	[14]
$(Al,Co,Fe,Va)_1$	$^0L_{Co,Va}^{A2} = +130988 - 11.39T$	This work
	$^0L_{Fe,Va}^{A2} = +150000$	This work
	$^0L_{Al,Co}^{A2} = -93092 + 1.3T$	This work
	$^0L_{Al,Fe}^{A2} = -122360+31.6T$	[17]
	$^1L_{Al,Fe}^{A2} = +2945.2$	[17]
	$^2L_{Al,Fe}^{A2} = +495$	[17]
	$^0T_{C_{Al,Fe}}^{A2} = -437.95$	[17]
	$^0T_{C_{Al,Fe}}^{A2} = -1719.7$	[17]
	$^0L_{Co,Fe}^{A2} = -20205 + 14.8T + 0.9845T\ln T - 0.0076434T^2$	[15]
	$^1L_{Co,Fe}^{A2} = +0$	[15]
	$^2L_{Co,Fe}^{A2} = +1316$	[15]
	$^0T_{C_{Co,Fe}}^{A2} = +590$	[15]
	$^0\beta_{Co,Fe}^{A2} = +1.5$	[15]
	$^1\beta_{Co,Fe}^{A2} = -0.6$	[15]
	$^0L_{Al,Co,Fe}^{A2} = {}^1L_{Al,Co,Fe}^{A2} = 0$	This work
	$^2L_{Al,Co,Fe}^{A2} = -30690.5 - 49.42T$	This work
B2	$^0G_{Al:Al}^{B2} = {}^0G_{Co:Co}^{B2} = {}^0G_{Fe:Fe}^{B2} = {}^0G_{Va:Va}^{B2} = 0$	This work
$(Al,Co,Fe,Va)_{0.5}(Al,Co,Fe,Va)_{0.5}$	$^0G_{Al:Va}^{B2} = {}^0G_{Va:Al}^{B2} = -70000 - 15.5T$	[14]
	$^0G_{Co:Va}^{B2} = {}^0G_{Va:Co}^{B2} = +20464 + 18.775T$	This work
	$^0G_{Fe:Va}^{B2} = {}^0G_{Va:Fe}^{B2} = 0$	This work
	$^0G_{Al:Co}^{B2} = {}^0G_{Co:Al}^{B2} = -92954+30.07T$	This work
	$^0G_{Al:Fe}^{B2} = {}^0G_{Fe:Al}^{B2} = -16072-4.56T$	[17]
	$^0T_{C_{Al:Fe}}^{B2} = {}^0T_{C_{Fe:Al}}^{B2} = -250$	[17]
	$^0\beta_{Al:Fe}^{B2} = {}^0\beta_{Fe:Al}^{B2} = -2.72$	[17]
	$^0G_{Co:Fe}^{B2} = {}^0G_{Fe:Co}^{B2} = -1245 - 1.89T$	[15]
	$^0T_{C_{Co:Fe}}^{B2} = {}^0T_{C_{Fe:Co}}^{B2} = +370$	[15]
	$^0\beta_{Co:Fe}^{B2} = {}^0\beta_{Fe:Co}^{B2} = +0.14$	[15]
	$^0L_{Al,Fe:Al}^{B2} = {}^0L_{Al:Al,Fe}^{B2} = 5600$	[17]

Table 6 continued

Phase	Parameter (J/mole per formula unit)	Reference
	$^0L^{B2}_{Al,Fe:Fe} = {}^0L^{B2}_{Fe:Al,Fe} = -1400+2.4T$	[17]
	$^0L^{B2}_{Al,Fe:Al,Fe} = -8400 - 4.8T$	[17]
	$^0L^{B2}_{Al,Fe:*} = {}^0L^{B2}_{*:Al,Fe} = -3946 - 4T$	[17]
	$^1L^{B2}_{Al,Fe:*} = {}^1L^{B2}_{*:Al,Fe} = +120$	[17]
	$^2L^{B2}_{Al,Fe:*} = {}^2L^{B2}_{*:Al,Fe} = -520$	[17]
	$^0T^{B2}_{C_{Al,Fe:*}} = {}^0T^{B2}_{C_{*:Al,Fe}} = +250$	[17]
	$^0\beta^{B2}_{Al,Fe:*} = {}^0\beta^{B2}_{*:Al,Fe} = -0.6$	[17]
	$^1\beta^{B2}_{Al,Fe:*} = {}^1\beta^{B2}_{*:Al,Fe} = -1.6$	[17]
	$^2\beta^{B2}_{Al,Fe:*} = {}^2\beta^{B2}_{*:Al,Fe} = +0.4$	[17]
	$^0L^{B2}_{Co,Fe:Fe} = {}^0L^{B2}_{Fe:Co,Fe} = -872$	[15]
	$^0T^{B2}_{C_{Co,Fe:Fe}} = {}^0T^{B2}_{C_{Fe:Co,Fe}} = {}^0T^{B2}_{C_{Co,Fe:Co}} = {}^0T^{B2}_{C_{Co:Co,Fe}} = -370$	[15]
	$^0L^{B2}_{Al,Co:Fe} = {}^0L^{B2}_{Fe:Al,Co} = -27277.6 + 15.31T$	This work
	$^1L^{B2}_{Al,Co:Fe} = {}^1L^{B2}_{Fe:Al,Co} = +20423.4 - 3.36T$	This work
	$^0L^{B2}_{Co,Fe:Al} = {}^0L^{B2}_{Al:Co,Fe} = +7176.5$	This work
	$^1L^{B2}_{Co,Fe:Al} = {}^1L^{B2}_{Al:Co,Fe} = -3399.6 + 2.50T$	This work
	$^0L^{B2}_{Al,Fe:Co} = {}^0L^{B2}_{Co:Al,Fe} = -6610.6 + 8.05T$	This work
	$^1L^{B2}_{Al,Fe:Co} = {}^1L^{B2}_{Co:Al,Fe} = -5000.5 + 2.51T$	This work
fcc	$^0L^{A1}_{Al,Co} = -124200 + 17.24T$	[14]
$(Al,Co,Fe)_1$	$^1L^{A1}_{Al,Co} = +6212.7 - 3.73T$	[14]
	$^2L^{A1}_{Al,Co} = +31337 - 1.56T$	[14]
	$^0T^{A1}_{C_{Al,Co}} = -1950$	[14]
	$^0\beta^{A1}_{Al,Co} = +6.98$	[14]
	$^0L^{A1}_{Al,Fe} = -100041 + 25.14T$	[17]
	$^1L^{A1}_{Al,Fe} = +33159 - 11.86T$	[17]
	$^2L^{A2}_{Al,Fe} = +32200 - 17T$	[17]
	$^0L^{A1}_{Co,Fe} = -9112 + 3.3T$	[15]
	$^1L^{A1}_{Co,Fe} = 0$	[15]
	$^2L^{A1}_{Co,Fe} = +1667$	[15]
	$^0T^{A1}_{C_{Co,Fe}} = +283$	[15]
	$^1T^{A1}_{C_{Co,Fe}} = +879$	[15]
	$^0\beta^{A1}_{Co,Fe} = +8.9$	[15]
	$^1\beta^{A1}_{Co,Fe} = -3.9$	[15]
	$^0L^{A1}_{Al,Co,Fe} = +201300$	This work
	$^1L^{A1}_{Al,Co,Fe} = +35490$	This work
	$^2L^{A1}_{Al,Co,Fe} = -75560$	This work

Table 6 continued

Phase	Parameter (J/mole per formula unit)	Reference
hcp	$^0L^{A3}_{Co,Fe} = -8500 + 7T$	[15]
$(Al,Co,Fe)_1$	$^1L^{A3}_{Co,Fe} = -800$	[15]
	$^0T^{A3}_{C_{Co,Fe}} = -253$	[15]
	$^1T^{A3}_{C_{Co,Fe}} = +1494$	[15]
	$^0\beta^{A3}_{Co,Fe} = -0.78$	[15]
	$^1\beta^{A3}_{Co,Fe} = +2.24$	[15]
$Al_5(Co,Fe)_2$	$^oG^{Al_5(Co,Fe)_2}_{Al:Co} - 5^oG^{A1}_{Al} - 2^oG^{A3}_{Co} = -329990 + 73.45T$	[14]
$(Al)_5(Co,Fe)_2$	$^oG^{Al_5(Co,Fe)_2}_{Al:Fe} - 5^oG^{A1}_{Al} - 2^oG^{A2}_{Fe} = -227000 + 54T$	[17]
	$^0L^{Al_5(Co,Fe)_2}_{Al:Co,Fe} = -108240.9 + 74.2T$	This work
	$^1L^{Al_5(Co,Fe)_2}_{Al:Co,Fe} = +36253.3$	This work
Al_3Co	$^oG^{Al_3Co}_{Al:Co} - 3^oG^{A1}_{Al} - ^oG^{A3}_{Co} = -165046 + 32.725T$	This work
$(Al)_3(Co)_1$		
$Al_{13}(Co,Fe)_4$	$^oG^{Al_{13}(Co,Fe)_4}_{Al:Fe:Al} - 0.765^oG^{A1}_{Al} - 0.235^oG^{A2}_{Fe} = -30680 + 7.44T$	[17]
$(Al)_{0.6275}(Co,Fe)_{0.235}(Al,Va)_{0.1375}$	$^oG^{Al_{13}(Co,Fe)_4}_{Al:Fe:Va} - 0.6275^oG^{A1}_{Al} - 0.235^oG^{A2}_{Fe} = -28100 + 7.44T$	[17]
	$^oG^{Al_{13}(Co,Fe)_4}_{Al:Co:Al} - 0.765^oG^{A1}_{Al} - 0.235^oG^{A3}_{Co} = -38800.588 + 7.36T$	This work
	$^oG^{Al_{13}(Co,Fe)_4}_{Al:Co:Va} - 0.6275^oG^{A1}_{Al} - 0.235^oG^{A3}_{Co} = -36000 + 11.8T$	This work
	$^0L^{Al_{13}(Co,Fe)_4}_{Al:Co,Fe:Al} = +1458$	This work
$Al_9(Co,Fe)_2$	$^oG^{Al_9(Co,Fe)_2}_{Al:Co} - 9^oG^{A1}_{Al} - 2^oG^{A3}_{Co} = -329700 + 53.14T$	[14]
$(Al)_9(Co, Fe)_2$	$^oG^{Al_9(Co,Fe)_2}_{Al:Fe} - 9^oG^{A1}_{Al} - 2^oG^{A2}_{Fe} = -175000$	This work
	$^0L^{Al_9(Co,Fe)_2}_{Al:Co,Fe} = -9158$	This work
Al_8Fe_5	$^oG^{Al_8Fe_5}_{Al:Al} - 13^oG^{A1}_{Al} = 0$	[17]
$(Al,Fe)_8(Al, Fe)_5$	$^oG^{Al_8Fe_5}_{Al:Fe} - 8^oG^{A1}_{Al} - 5^oG^{A2}_{Fe} = -394000 + 36.2T$	[17]
	$^oG^{Al_8Fe_5}_{Fe:Al} - 5^oG^{A1}_{Al} - 8^oG^{A2}_{Fe} = +200000 + 36.2T$	[17]
	$^oG^{Al_8Fe_5}_{Fe:Fe} - 13^oG^{A2}_{Fe} = +13000$	[17]
	$^0L^{Al_8Fe_5}_{Al:Al,Fe} = -120000$	[17]
	$^0L^{Al_8Fe_5}_{Al,Fe:Fe} = -174000$	[17]
$Al_2(Co,Fe)$	$^oG^{Al_2(Co,Fe)}_{Al:Fe} - 2^oG^{A1}_{Al} - ^oG^{A2}_{Fe} = -103900 + 23T$	[17]
$(Al)_2(Co,Fe)_1$	$^oG^{Al_2(Co,Fe)}_{Al:Co} - 2^oG^{A1}_{Al} - ^oG^{A3}_{Co} = -102030 + 10T$	This work
	$^oG^{Al_2(Co,Fe)}_{Al:Co,Fe} = -53177.2 + 24.8T$	This work

Figure 5 Calculated Co-Al phase diagram using the modified thermodynamic parameters.
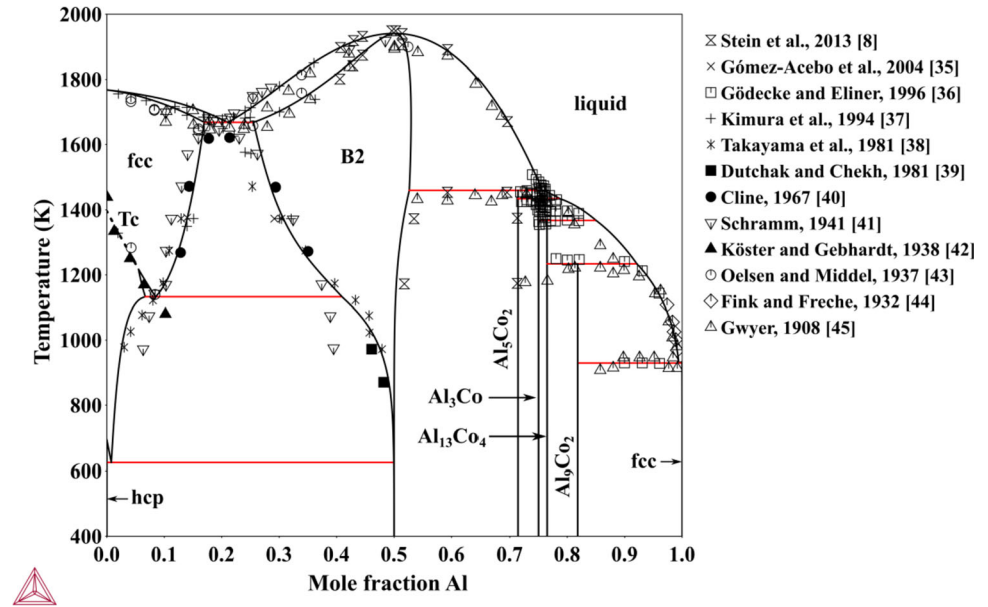
the thermodynamic description of the Al–Fe system, as shown in Fig. 9a. Moreover, although the difference in the Al content was very small in Fig. 9b and c, the difference in the liquidus temperature was more than 20 K.

Atomic mobility assessment

The atomic mobilities of the fcc Co-Al–Fe alloys were optimized based on the interdiffusion coefficients determined in this study. The mobilities for the binary sub-systems were directly taken from Refs. [14, 15, 24, 25] as mentioned in "Diffusion data" Section. Mobility interaction parameters were introduced to improve the fitting of the experimental data. Table 7 summarizes the atomic mobility parameters. A comparison of the logarithmic values of the calculated main interdiffusion coefficients with the experimental data is shown in Fig. 10. The dashed lines form a generally accepted error band of a multiplying factor of 2.0 or 0.5. The calculated main interdiffusion coefficients are in reasonable agreement with the corresponding experimental results determined in this study.

To validate the reliability of the present model parameters, a comparison between the calculated and experimental composition profiles of typical diffusion couples is shown in Figs. 11, 12 and 13. The experimental diffusion profiles were satisfactorily reproduced using the model parameters. As observed, the diffusion of Al was slightly faster than that of Fe, which indicates that the interdiffusion coefficient of Al is larger than that of Fe in fcc Co-Al–Fe alloys.

The calculated diffusion paths of all the diffusion couples were compared with the experimental data, as shown in Fig. 14, and good agreement was observed. The diffusion paths show a slightly curved S shape, which is caused by the difference in the interdiffusion coefficient and the mass balance of the diffusion species [52].

Summary

In the present work, the thermodynamic parameters of the Co-Al–Fe system and atomic mobilities for the fcc phase were successfully assessed using the

CALPHAD method based on experimental data from the present work and literature.

The Al-rich side phase boundary of the B2 phase at 1273 and 1343 K was determined by EPMA and XRD. The phase equilibria between the B2 and intermetallic compounds were established, and no new ternary compounds were identified. Moreover, the phase equilibria at the Co-Fe rich side at 1073 K were carefully established. The miscibility gap of the B2

phase at 1073 K was not observed. Only a A2/B2 order–disorder transformation was observed. Combined with the previous experimental work and the data in the literature, the thermodynamic description of the Co-Al–Fe system was critically assessed. The present thermodynamic description can reasonably reproduce reliable experimental data.

The interdiffusion coefficients in the fcc phase were experimentally investigated at 1323, 1423, and 1523 K using the diffusion couple method. Combined with the present thermodynamic description, the atomic mobilities of Co, Al, and Fe in fcc Co-Al–Fe alloys were assessed. Comprehensive comparisons between the calculated and experimental diffusion profiles and paths indicated that the diffusion behavior was
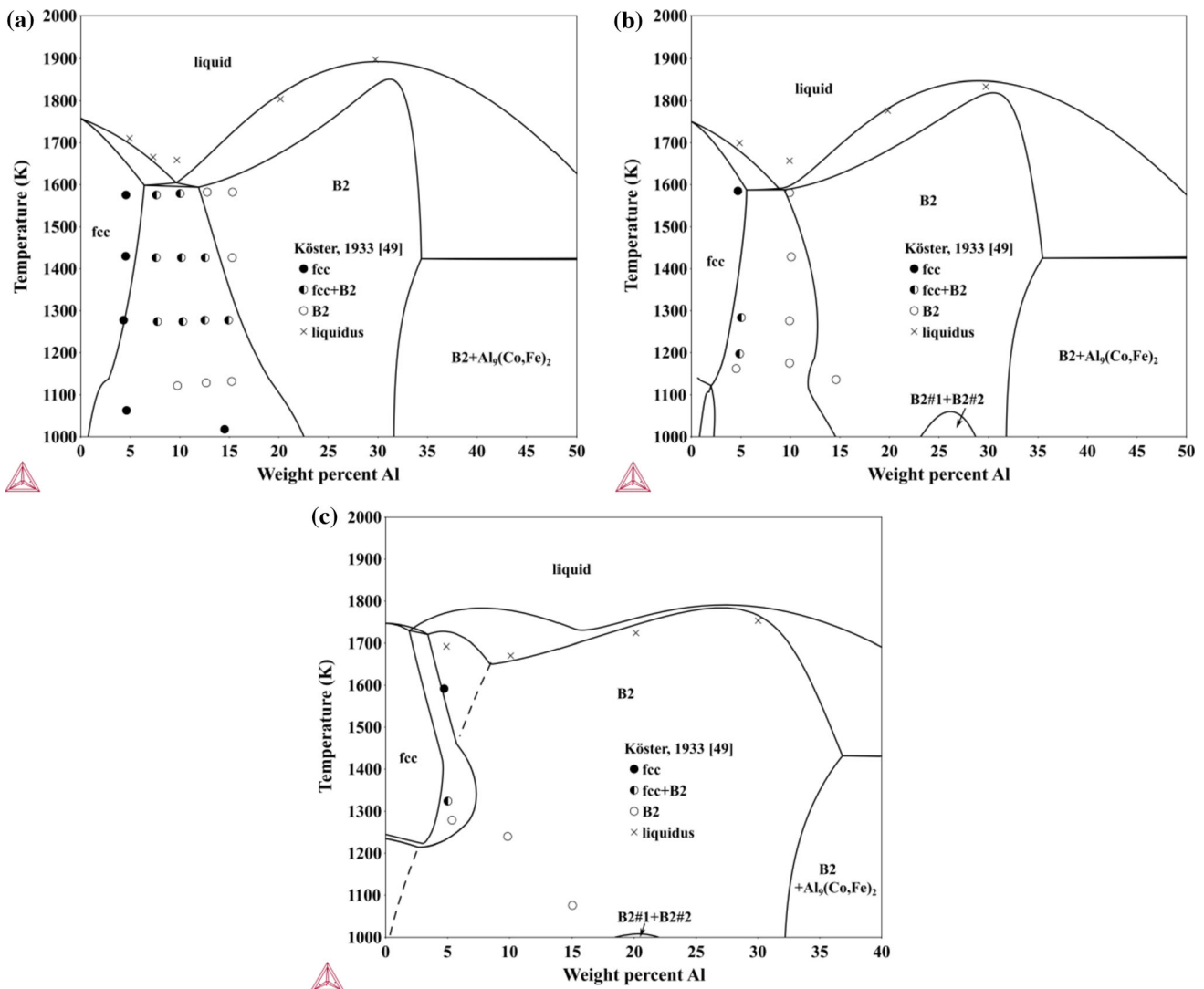
Figure 7 Calculated isoplethal section of the Co-Al–Fe system in comparison with experimental data: **a** 10 wt.% Fe, **b** 20 wt.% Fe, and **c** 40 wt.% Fe. The dashed line represents the A2/B2 second-order transition.
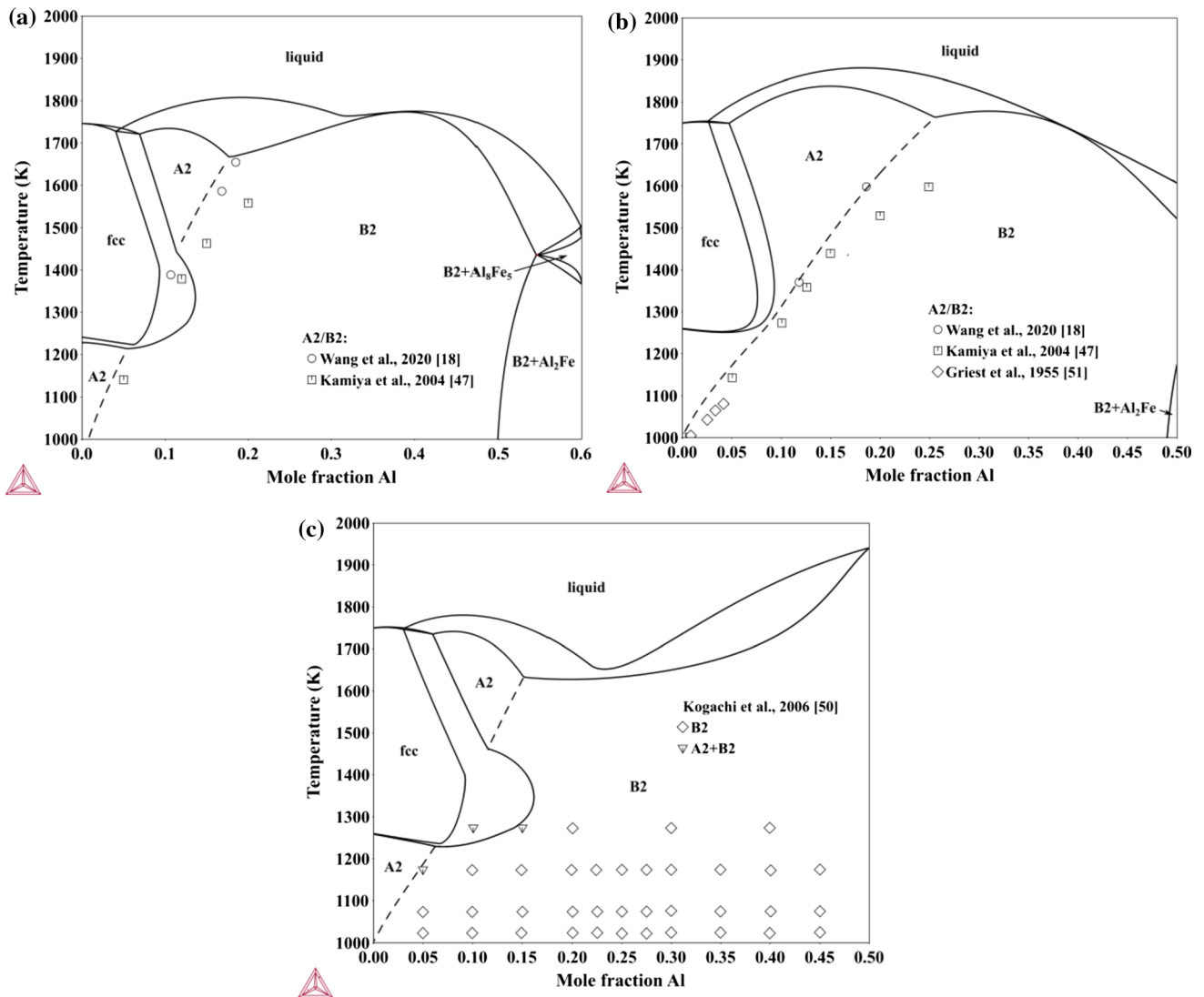
Figure 8 Calculated isoplethal sections of the Co-Al–Fe system in comparison with experimental data: **a** 40 at.% Fe, **b** 50 at.% Fe, and **c** 50 at.% Co. Dashed lines represent the A2/B2 order–disorder transition.
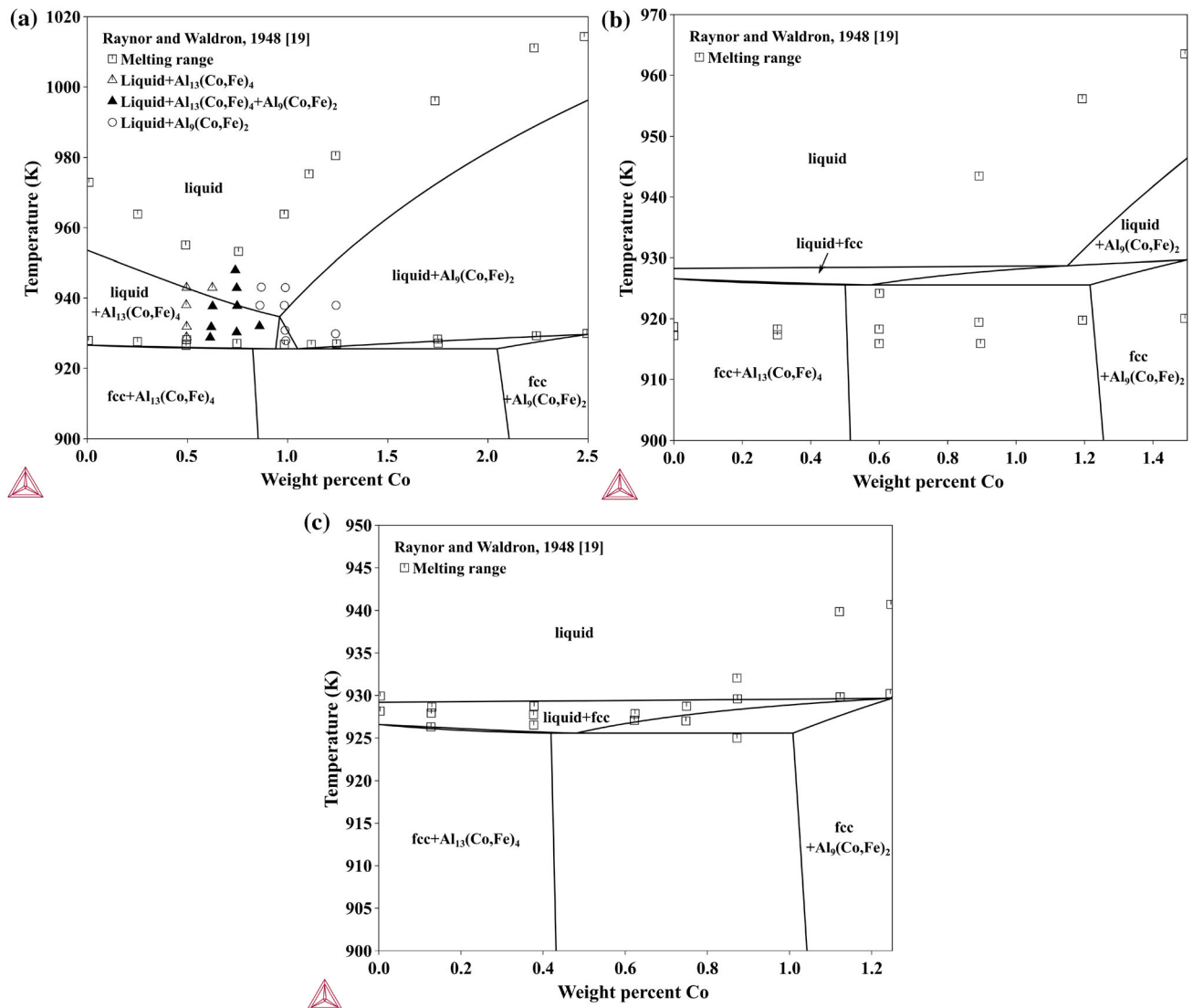
Figure 9 Calculated isoplethal sections of the Co-Al–Fe system at the Al-rich corner in comparison with experimental data: **a** 97.5 wt.% Al, **b** 98.5 wt.% Al, and **c** 98.75 wt.% Al.

Table 7 Summary of the atomic mobilities for fcc Co-Al–Fe alloys

Mobility	Parameter (J/mol)
Mobility of Al	
Q_{Al}^{Al}	$26719 + R \times T \times \mathrm{LN}(1.08 \times 10^{-5})$
Q_{Al}^{Co}	$-275359 + R \times T \times \mathrm{LN}(1.54 \times 10^{-4})$
Q_{Al}^{Fe}	$-242731.1 + R \times T \times \mathrm{LN}(3.575 \times 10^{-6})$
$^{0}Q_{Al}^{Al,Co}$	$+50000$
$^{0}Q_{Al}^{Co,Fe}$	-6047.9
Mobility of Co	
Q_{Co}^{Al}	$-172082 + R \times T \times \mathrm{LN}(3.28 \times 10^{-2})$
Q_{Co}^{Co}	$-301654 + R \times T \times \mathrm{LN}(2.18 \times 10^{-4})$
Q_{Co}^{Fe}	$-301900 + R \times T \times \mathrm{LN}(1.0 \times 10^{-4})$
$^{0}Q_{Co}^{Al,Co}$	-50000
$^{0}Q_{Co}^{Co,Fe}$	$+315049 - 218.5 \times T$
Mobility of Fe	
Q_{Fe}^{Al}	$-214000 + R \times T \times \mathrm{LN}(3.62 \times 10^{-1})$
Q_{Fe}^{Co}	$-259074 + R \times T \times \mathrm{LN}(1.61 \times 10^{-5})$
Q_{Fe}^{Fe}	$-286000 + R \times T \times \mathrm{LN}(7.0 \times 10^{-5})$
$^{0}Q_{Fe}^{Co,Fe}$	$-61585 + 51.88 \times T$
$^{0}Q_{Fe}^{Al,Co}$	-111270
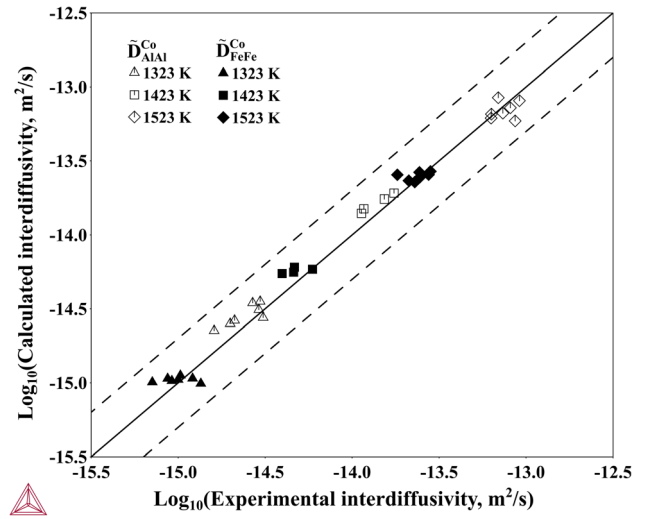
Figure 10 Comparison between the presently calculated and the experimental main diffusion coefficients in fcc Co-Al–Fe alloys.
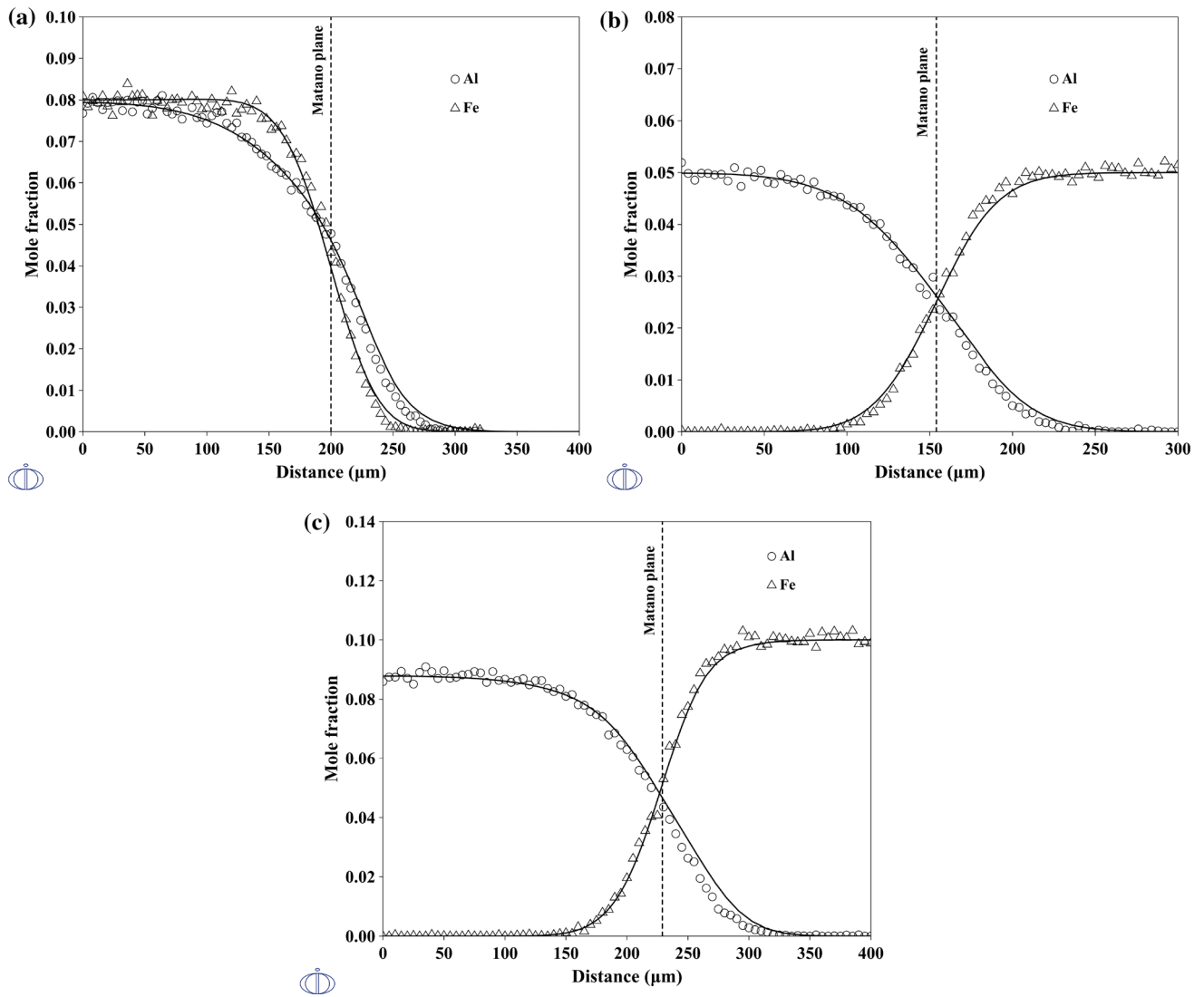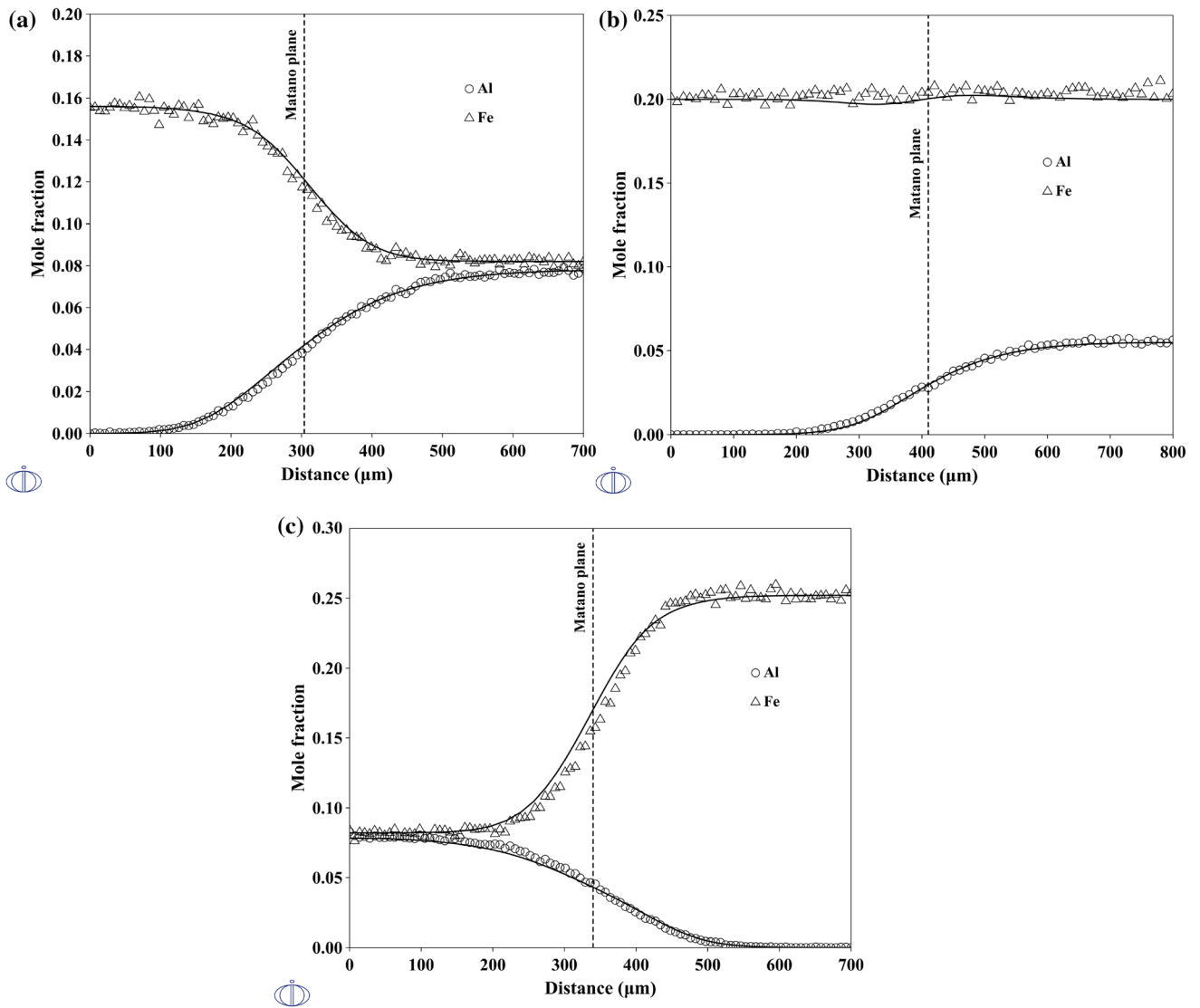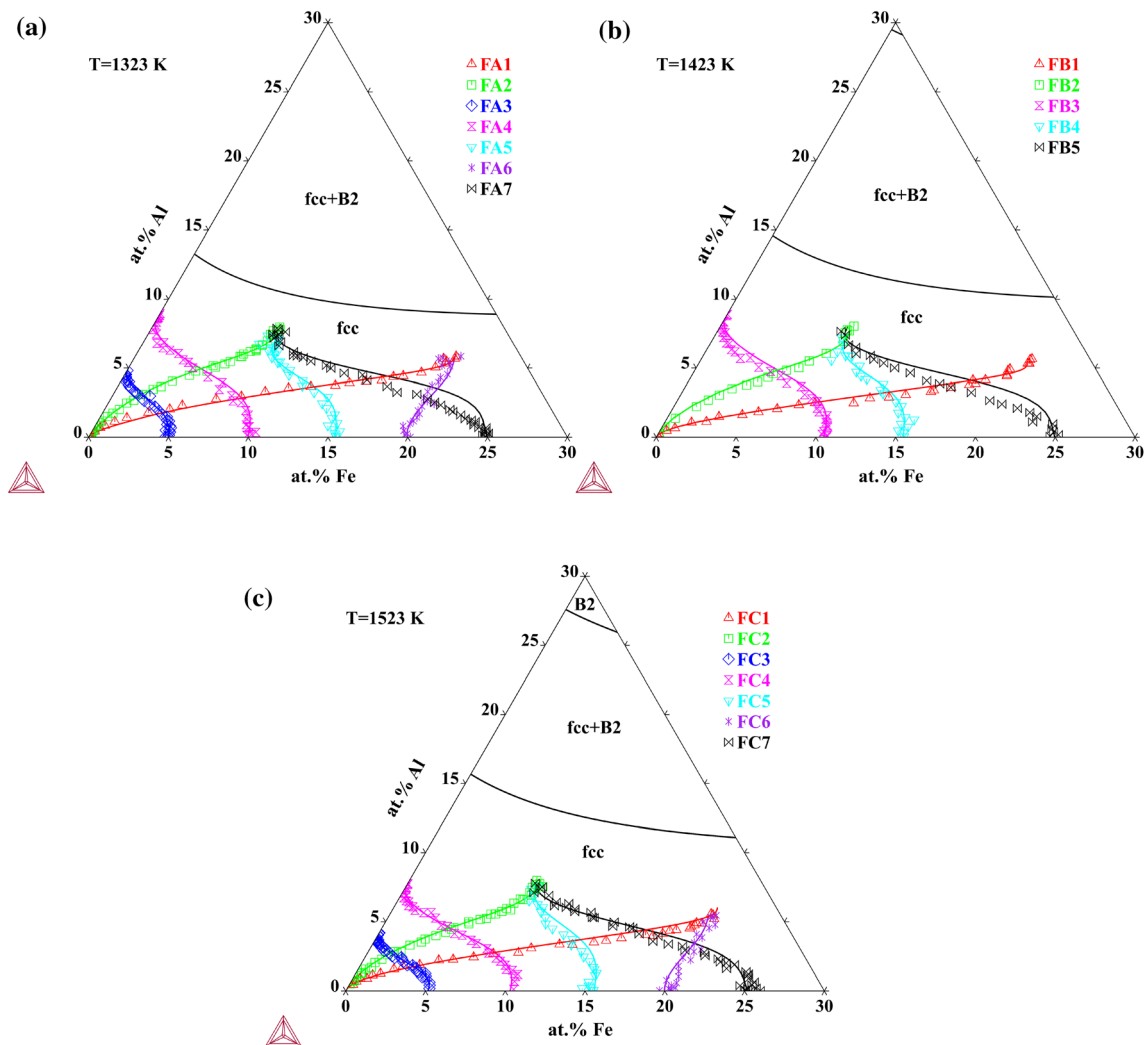
Figure 11 Comparison between the calculated and measured concentration profiles for the diffusion couples annealed at 1323 K for 120 h: (a) FA2, (b) FA3, and (c) FA4.
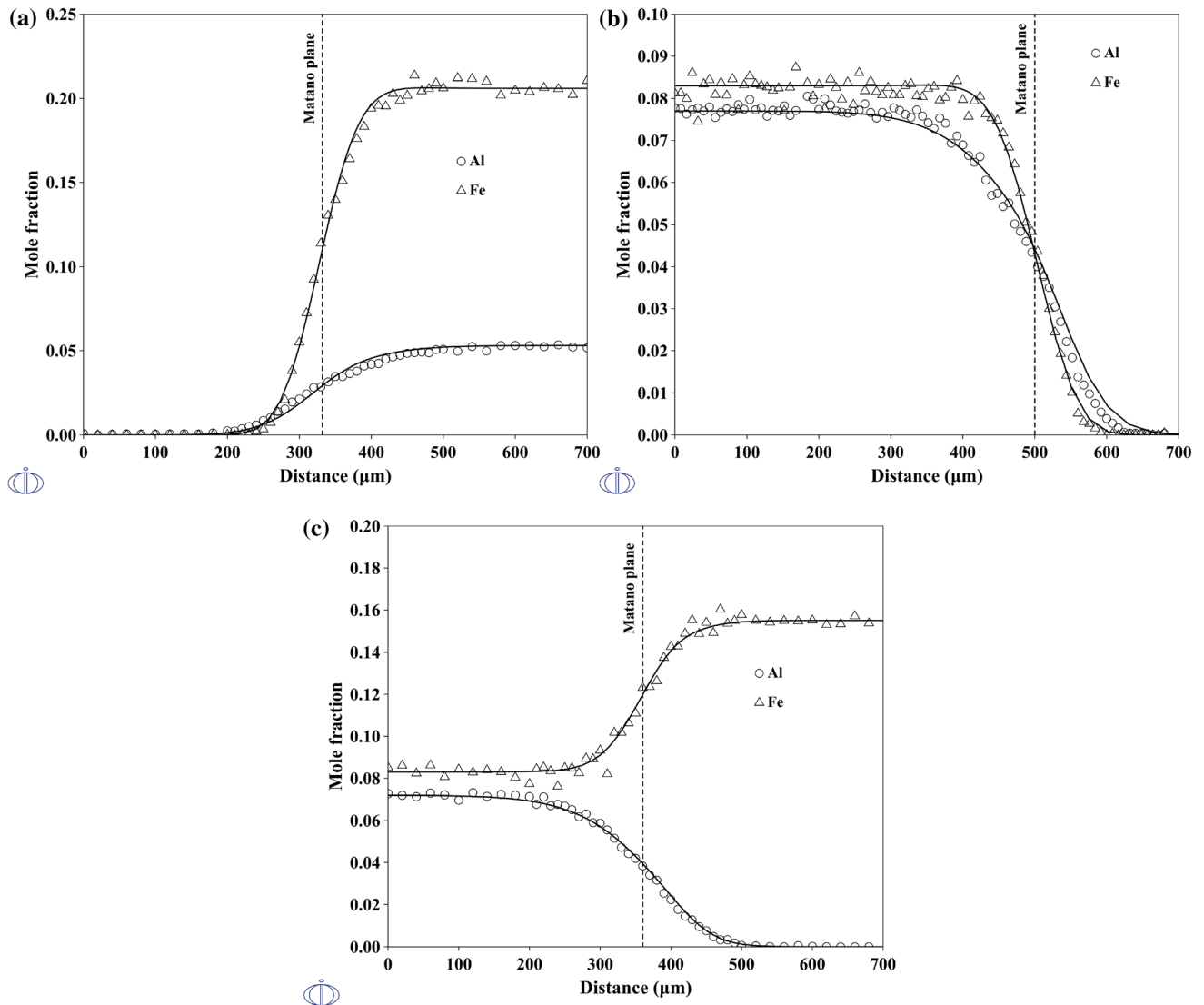
Figure 12 Comparison between the calculated and measured concentration profiles for the diffusion couples annealed at 1423 K for 48 h: (a) FB1, (b) FB2, and (c) FB4.

Figure 13 Comparison between the calculated and measured concentration profiles for the diffusion couples annealed at 1523 K for 24 h: (a) FC5, (b) FC6, and (c) FC7.

Figure 14 Comparison between the calculated diffusion paths and the experimental data of the ternary fcc Co–Al–Fe diffusion couples annealed at (a) 1323 K, (b) 1423 K, and (c) 1523 K.

adequately represented by the present mobility description.

Declarations

Conflict of interest The authors declare that they have no conflicts of interest.

Supplementary Information: The online version contains supplementary material available at http s://doi.org/10.1007/s10853-022-07109-8.

References

[1] Yeh J-W, Chen S-K, Lin S-J et al (2004) Nanostructured high-entropy alloys with multiple principal elements: novel alloy design concepts and outcomes. Adv Eng Mater 6:299–303. https://doi.org/10.1002/adem.200300567

[2] Zhou YJ, Zhang Y, Wang YL, Chen GL (2007) Solid solution alloys of AlCoCrFeNiTix with excellent room-temperature mechanical properties. Appl Phys Lett 90:181904. https://doi.org/10.1063/1.2734517

[3] Lu Y, Dong Y, Guo S et al (2015) A promising new class of high-temperature alloys: eutectic high-entropy alloys. Sci Rep 4:6200. https://doi.org/10.1038/srep06200

[4] Lu Y, Gao X, Jiang L et al (2017) Directly cast bulk eutectic and near-eutectic high entropy alloys with balanced strength and ductility in a wide temperature range. Acta Mater 124:143–150. https://doi.org/10.1016/j.actamat.2016.11.016

[5] Gao X, Lu Y, Zhang B et al (2017) Microstructural origins of high strength and high ductility in an AlCoCrFeNi2.1 eutectic high-entropy alloy. Acta Mater 141:59–66. https://doi.org/10.1016/j.actamat.2017.07.041

[6] Dupin N, Ansara I (1998) Thermodynamic assessment of the system Al-Co. Revue de Metallurgie 95:1121–1129

[7] Ohtani H, Chen Y, Hasebe M (2004) Phase separation of the B2 structure accompanied by an ordering in Co-Al and Ni-Al binary systems. Mater Trans 45:1489–1498. https://doi.org/10.2320/matertrans.45.1489

[8] Stein F, He C, Dupin N (2013) Melting behaviour and homogeneity range of B2 CoAl and updated thermodynamic description of the Al–Co system. Intermetallics 39:58–68. https://doi.org/10.1016/j.intermet.2013.03.011

[9] Liu XL, Gheno T, Lindahl BB et al (2015) First-principles calculations, experimental study, and thermodynamic modeling of the Al-Co-Cr system. PLoS ONE 10:e0121386. https://doi.org/10.1371/journal.pone.0121386

[10] Wang P, Xiong W, Kattner UR et al (2017) Thermodynamic re-assessment of the Al-Co-W system. Calphad 59:112–130. https://doi.org/10.1016/j.calphad.2017.09.007

[11] Wang Y, Cacciamani G (2018) Experimental investigation and thermodynamic assessment of the Al-Co-Ni system. Calphad 61:198–210. https://doi.org/10.1016/j.calphad.2018.03.008

[12] Ostrowska M, Cacciamani G (2019) Critical evaluation and thermodynamic modeling of the Al-Co-Fe system. J Alloy Compd 794:553–568. https://doi.org/10.1016/j.jallcom.2019.04.170

[13] Noori M, Hallstedt B (2020) Thermodynamic modelling of the Al–Co–Mn system. Calphad 71:101793. https://doi.org/10.1016/j.calphad.2020.101793

[14] Wang Y (2018) Study on the thermodynamics of the Ni-Co-Al-Mo-W system and the diffusion kinetics of its fcc phase Ph.D. thesis, Shanghai University

[15] Wang J, Lu X-G, Zhu N, Zheng W (2017) Thermodynamic and diffusion kinetic studies of the Fe-Co system. Calphad 58:82–100. https://doi.org/10.1016/j.calphad.2017.06.001

[16] Sundman B, Ohnuma I, Dupin N et al (2009) An assessment of the entire Al–Fe system including D03 ordering. Acta Mater 57:2896–2908. https://doi.org/10.1016/j.actamat.2009.02.046

[17] Zheng W, He S, Selleby M et al (2017) Thermodynamic assessment of the Al-C-Fe system. Calphad 58:34–49. https://doi.org/10.1016/j.calphad.2017.05.003

[18] Wang J, Zheng W, Lu X et al (2020) Experimental study of phase equilibria on Co–Fe-rich side of Co–Al–Fe system. J Iron Steel Res Int 27:673–680. https://doi.org/10.1007/s42243-019-00336-5

[19] Raynor GV, Waldron MB (1948) The constitution of the aluminium-rich aluminium-cobalt-iron alloys, with reference to the role of transitional elements in alloy formation Proceedings of the Royal Society of London Series A Mathematical and Physical Sciences 194:362–374 https://doi.org/10.1098/rspa.1948.0086

[20] Ackermann H (1988) Experimentelle Untersuchung und Monte-Carlo-Simulation chemischer Ordnungsreaktionen in den ternären kubisch raumzentrierten Fe–Co–Al Legierungen. Ph.D. thesis, Universität Dortmund

[21] Zhu L, Soto-Medina S, Hennig RG, Manuel MV (2020) Experimental investigation of the Al–Co–Fe phase diagram over the whole composition range. J Alloy Compd 815:152110. https://doi.org/10.1016/j.jallcom.2019.152110

[22] Grushko B, Kowalski W, Surowiec M (2010) On the constitution of the Al–Co–Fe alloy system. J Alloy Compd 491:L5–L7. https://doi.org/10.1016/j.jallcom.2009.10.156

[23] Noori M, Hallstedt B (2021) Thermodynamic modelling of the Al–Co–Fe system. Calphad 74:102288. https://doi.org/10.1016/j.calphad.2021.102288

[24] Du Y, Chang YA, Huang B et al (2003) Diffusion coefficients of some solutes in fcc and liquid Al: critical evaluation and correlation. Mater Sci Eng A 363:140–151. https://doi.org/10.1016/S0921-5093(03)00624-5

[25] Liu D, Zhang L, Du Y et al (2013) Development of an atomic mobility database for disordered and ordered fcc phases in multicomponent Al alloys: focusing on binary systems. Int J Mater Res 104:135–148. https://doi.org/10.3139/146.110846

[26] Redlich O, Kister AT (1948) Algebraic representation of thermodynamic properties and the classification of solutions. Ind Eng Chem 40:345–348. https://doi.org/10.1021/ie50458a036

[27] Inden G (1981) The role of magnetism in the calculation of phase diagrams Physica B+C 103: 82–100 https://doi.org/10.1016/0378-4363(81)91004-4

[28] Hillert M, Jarl M (1978) A model for alloying in ferromagnetic metals. Calphad 2:227–238. https://doi.org/10.1016/0364-5916(78)90011-1

[29] Ansara I, Dupin N, Lukas HL, Sundman B (1997) Thermodynamic assessment of the Al-Ni system. J Alloy Compd 247:20–30. https://doi.org/10.1016/S0925-8388(96)02652-7

[30] Kozakai T, Okamoto R, Miyazaki T (1999) Phase equilibria in the Fe-Al-Co ternary system at 923 K. Z Met 90:261–266

[31] Andersson J, Ågren J (1992) Models for numerical treatment of multicomponent diffusion in simple phases. J Appl Phys 72:1350–1355. https://doi.org/10.1063/1.351745

[32] Whittle DP, Green A (1974) The measurement of diffusion coefficients in ternary systems. Scr Mater 8:883–884

[33] Edwards OS (1941) An X-ray investigation of the aluminium-cobalt-iron system. J Jpn Instit Metal 67:67–77

[34] Kirkaldy JS, Weichert D, Haq Z-U (1963) Diffusion in multicomponent metallic systems: VI. some thermodynamic properties of the D matrix and the corresponding solutions of the diffusion equations. Can J Phys 41:2166–2173

[35] Gómez-Acebo T, Navarcorena B, Castro F (2004) Interdiffusion in multiphase, Al-Co-Cr-Ni-Ti diffusion couples. J Phase Equilib Diffus 25:237–251. https://doi.org/10.1007/s11669-004-0112-y

[36] Gödecke T, Eliner M (1996) Phase equilibria in the aluminium-rich portion of the binary system Co-Al and in the cobalt/aluminium-rich portion of the ternary system Co-Ni-Al. Int J Mater Res 87:854–864. https://doi.org/10.1515/ijmr-1996-871107

[37] Kimura Y, Kuriyama H, Suzuki T, Mishima Y (1994) Microstructure control and mechanical properties of binary Co-Al alloys based on B2 intermetallic compound CoAl. Mater Trans JIM 35:182–188. https://doi.org/10.2320/matertrans1989.35.182

[38] Takayama T, Wey MY, Nishizawa T (1981) Effect of magnetic transition on the solubility of alloying elements in cobalt. J Jpn Inst Met 22:315–325. https://doi.org/10.2320/matertrans1960.22.315

[39] Dutchak YI, Chekh VG (1981) High temperature X-ray diffraction study of the lattice dynamics of the compounds AlCo and AlNi. Russ J Phys Chem 55:1326–1328

[40] Cline HE (1967) The mechanical properties of the CoAl-Co eutectic. Transaction Metallur Soc AIME 239:1906–1916

[41] Schramm J (1941) Das binäre Teilsystem Nickel-NiAl. Int J Mater Res 33:347–355. https://doi.org/10.1515/ijmr-1941-331004

[42] Köster W, Gebhardt E (1938) Das system Kobalt-Mangan-aluminium. Int J Mater Res 30:281–286. https://doi.org/10.1515/ijmr-1938-300901

[43] Oelsen W, Middel W (1937) Mitt. Kaiser-Wilhelm Inst Eisenforsch Düsseldorf 19:1–26

[44] Fink W, Freche H (1932) Equilibrium relation in aluminum-cobalt alloys of high purity. Transaction Am Inst Min Metallur Petroleum Eng (AIME) 99:141–148

[45] Gwyer AGC (1908) über die Legierungen des Aluminiums mit Kupfer, Eisen, Nickel, Kobalt, Blei und Cadmium. Z Anorg Chem 57:113–153. https://doi.org/10.1002/zaac.19080570106

[46] Andersson J-O, Helander T, Höglund L et al (2002) Thermo-Calc & DICTRA, computational tools for materials science. Calphad 26:273–312. https://doi.org/10.1016/S0364-5916(02)00037-8

[47] Kamiya N, Sakai T, Kainuma R et al (2004) Phase separation of BCC phase in the Co-rich portion of Co-Fe-Al system. Intermetallics 12:417–423. https://doi.org/10.1016/j.intermet.2003.12.005

[48] Rusina NE, Kalmykov KB, Dunaev SF (1996) Interaction of elements in the system Al-Fe-Co at 1400 K Vestnik Moskovskogo Universiteta Seriya Khimiya 473–477

[49] Köster W (1933) Das system eisen-kobalt-aluminium. Archiv für das Eisenhüttenwesen 7:263–264. https://doi.org/10.1002/srin.193300046

[50] Kogachi M, Tadachi N, Nakanishi T (2006) Structural properties and magnetic behavior in CoFe1−xAlx alloys. Intermetallics 14:742–749. https://doi.org/10.1016/j.intermet.2005.11.006

[51] Griest AJ, Libsch JF, Conard GP (1955) Effect of ternary additions of silicon and aluminum on the ordering reaction in iron-cobalt. Acta Metall 3:509–510

[52] Sohn YH, Dayananda MA (2000) A double-serpentine diffusion path for a ternary diffusion couple. Acta Mater 48:1427–1433. https://doi.org/10.1016/S1359-6454(99)00454-1